New Two-layer Ruddlesden-popper Cathode Materials for Protonic Ceramics Fuel Cells

Y.H. Ling (lyhyy@cumt.edu.cn)
School of Materials Science and Physics, China University of Mining and Technology, Xuzhou 221116, P.R. China

Yihan Ling
China University of Mining and Technology - Xuzhou Campus: China University of Mining and Technology

Tianming Guo
China University of Mining and Technology

Yangyang Guo
China University of Mining and Technology

Yang Yang
China University of Mining and Technology

Yunfeng Tian
China University of Mining and Technology

Xinxin Wang
China University of Mining and Technology

Xuemei Ou
China University of Mining and Technology

Peizhong Feng
China University of Mining and Technology

Research Article

Keywords: Protonic ceramics fuel cells, Ruddlesden-Popper phase, single-phase cathode, Relaxation time distribution function, Charge transfer

Posted Date: February 9th, 2021

DOI: https://doi.org/10.21203/rs.3.rs-199356/v1

Abstract

New two-layer Ruddlesden-popper (RP) oxide $La_{0.25}Sr_{2.75}FeNiO_{7-\delta}$ (LSFN) in the combination of $Sr_3Fe_2O_{7-\delta}$ and $La_3Ni_2O_{7-\delta}$ was successfully synthesized and studied as the potential active single-phase and composite cathode for protonic ceramics fuel cells (PCFCs). LSFN with the tetragonal symmetrical structure (I4/mmm) is confirmed, and the co-existence of Fe^{3+} /Fe^{4+} and Ni^{3+}/Ni^{2+} couples is demonstrated by XPS analysis. The LSFN conductivity is apparently enhanced after Ni doping in Fe-site, and nearly three times those of $Sr_3Fe_2O_{7-\delta}$, which is directly related to the carrier concentration and conductor mechanism. Importantly, anode supported PCFCs using LSFN-BZCY composite cathode achieved high power density (426 mW·cm^{-2} at 650°C) and low electrode interface polarization resistance (0.26 Ω cm^2). Besides, relaxation time distribution function (DRT) technology was further used to analysis the electrode polarization processes. The observed three peaks (P1, P2, P3) separated by DRT shifted to the high frequency region with the decreasing temperature, suggesting that the charge transfer at the electrode-electrolyte interfaces become more difficult at reduced temperature. Preliminary results demonstrate new two-layer PR phase LSFN can be a promising cathode candidate for PCFCs.

1. Introduction

Protonic ceramics fuel cells (PCFCs) possess several advantages of high proton conductivity electrolytes with low activation energy and high fuel efficiency, receiving more attractive at reduced operating temperature [1–4]. However, As the temperature reduced, the corresponding challenge for the oxygen reduction reaction is the reduced cathodic catalytic activity, causing the large electrode polarization loss and fast degradation of cell performance [5–7]. Therefore, great efforts have been devoted to developing new cathode materials and modifying high performance conventional cathode materials that can own high catalytic activity at reduced temperature.

New cathodes with mixed conductivity based on simple perovskite (doped $LaCoO_3$, $BaCoO_3$ and $LaFeO_3$) have been extensively studied [7–12]. Considering high oxygen-ion defect concentration, oxygen diffusion anisotropy and cation ordered-structure, several recent studies have highlighted the promising of the Ruddlesden-Popper (RP) series, $A_{n+1}BnO_{3n+1}$, for cathode application, where the special sandwich structure consists of n ABO_3 perovskite and two AO rock salt layers[13–17]. The $Sr_3Fe_2O_{7-\delta}$-based systems, belonging to the n = 2 series, have been widely investigated owing to their high oxygen deficiency, excellent water-intercalation property and prominent catalytic activity [18–20]. The partial substitution of Ni for Fe in $Sr_3Fe_2O_{7-\delta}$ can increase the electrical conductivity and the oxygen permeability without structural transformation [21–22]. In our previous works, the introduction of La into Sr-site forming $La_xSr_{3-x}Fe_2O_{7-\delta}$ can enhance thermo-chemical stability as well as large oxygen deficiency [23–24]. Moreover, another RP phase, $La_3Ni_2O_{7-\delta}$ (n = 2), showed large electrical conductivity, acceptable stability and similar thermal expansion coefficient to electrolytes [25–27]. Therefore, in this work, we combine two RP phase oxides of $Sr_3Fe_2O_{7-\delta}$ and $La_3Ni_2O_{7-\delta}$ thanks to their similar ionic radii and chemical properties, expecting to enhance the conductivity and electrochemical activity without structural

transformation. Here, $La_{0.25}Sr_{2.75}FeNiO_{7-\delta}$ (LSFN) was successfully prepared and investigate the electrochemical performance to verify the possibility for using as cathode material for PCFCs. In addition, LSFN incorporated with BZCY to form a composite cathode for PCFCs were also examined. The polarization processes for PCFCs under working condition were detailly analyzed by relaxation time distribution function (DRT) method.

2. Experimental

LSFN, NiO-$BaZr_{0.1}Ce_{0.7}Y_{0.2}O_{3-\delta}$ (BZCY), and BZCY powders were synthesized by EDTA- citric acid combustion method, and the primary powders were calcined at 1200°C, 1100°C and 1100°C for 3 h, respectively [28]. X-ray diffraction (XRD) was used to perform all prepared powders as well as LSFN-BZCY mixtures calcined at different temperatures. X-ray photoelectron spectrometer (XPS) was used to analyze the elemental chemical state of LSFN, and then the conductivity measurement by H.P. multimeter using the standard DC four-probe technique was investigated from 800 to 300°C in air.

Anode supported PCFCs with LSFN single-phase and composite cathode were used to investigate the electrochemical performance. The NiO-BZCY-starch / NiO-BZCY / BZCY anode supported half cells were prepared by the dry pressing, and then sintering at 1400°C for 3h. Finally, LSFN and LSFN-BZCY (7:3) cathode slurry were brushed onto BZCY electrolyte surface severally, and then calcined at 900°C for 3 h in air. Anode supported PCFCs were evaluated by cell-testing system with humidified (~3% H_2O) H_2 fuel at 650°C-500°C. The impedance spectra (Chi604E, Shanghai Chenhua) under open-current conditions were investigated with the frequency range of 100kHz-0.01Hz and AC amplitude of 10mV at 650°C-500°C, of which the microstructure was performed using scanning electron microscopy (SEM).

3. Result And Discussion

XRD pattern of prepared LSFN powder was presented in Fig. 1(a), which clearly shows defined the tetragonal symmetry with the space group of I4/mmm in the light of standard powder diffraction information for $Sr_3Fe_2O_{7-\delta}$, indicating that the partial replacement of Fe with Ni can't affect the single RP phase structure [18-20]. Rietveld analysis (GSAS) was performed and the XRD Rietveld refinement results are also given in Fig. 1(a) and Fig. 1(b) (magnified results with 2θ of 25-50 °), where low refinement reliability factors (wRp=12.90%, Rp=9.84%, χ^2=2.05) were obtained. The calculated lattice parameters a and c based on this model are 3.8364(50) and 20.0376(93) Å, respectively, and one can clearly be seen that two perovskite layers are sandwiched by the rock-salt layer along the c-axis in the typical two-layer RP phase structure sandwiched as illustrated in Fig. 1(c) . In addition, LSFN sample with high crystallinity and well-defined crystalline fringes was observed in Fig. 1(d), and the lattice spacing of 0.2658nm corresponds to the lattice spacing of the (110) plane in the tetragonal symmetry in selected-angle diffraction in Fig. 1(b). All results together demonstrate the well maintained single RP phase structure after the combination of two RP phase oxides of $Sr_3Fe_2O_{7-\delta}$and $La_3Ni_2O_{7-\delta}$.

The elemental chemical state was characterized by XPS, and La3d, Sr3d, Fe2p and Ni2p peaks in XPS spectra for LSFN sample at room temperature were shown in Fig. 2. The peaks of binding energies of La 3d5/2 (at 834.4 and 838.1 eV) and La3d 3/2(at 851.5 eV) represent La^{3+} as revealed in Fig. 2(a). Fig. 2(b) proves Sr in LSFN sample displays a +2 valence state with the binding energies of Sr 3d5/2 (at 132.8 eV) and Sr 3d 3/2 (at 134.6 eV). Fig. 2(c) shows the Fe 2p binding energy region of LSFN sample, where the location of 710.5/724.1 eV and 712.5/725.9 eV peaks are related to the Fe2p 3/2 /Fe2p 1/2 signals for Fe^{3+} and Fe^{4+}, respectively, and the proportion of Fe^{4+} /Fe^{3+} is about 0.898 without the peaks of Fe^{2+} [29-30]. Fig. 2(d) reports the Ni 2p XPS spectra of LSFN sample, and the Ni 2p peaks that envelope the Ni^{2+} and Ni^{3+} valence states are fitted. One can clearly observed that four characteristic peaks with the binding energy of 855.8, 862.7, 873.5 and 880.5 eV, which related to Ni^{3+} 3d 5/2 and 3d 3/2, respectively, while the peaks of 2p 1/2 at 872.1 and 877.8 eV and 2p 3/2 at 854.4 and 860.7 eV can be attributed to Ni^{2+}, where the proportion of Ni^{3+} /Ni^{2+} is about 1.25[31-33]. The XPS results conform the fact that Fe^{3+}/Fe^{4+} and Ni^{3+}/Ni^{2+} couples are co-existed in the LSFN sample. Moreover, the conductivity of LSFN can be considered to be affected in LSFN sample as follows:

$$Fe^{4+} + Ni^{2+} \leftrightarrow Fe^{3+} + Ni^{3+} \quad (1)$$

Therefore, the introduction Ni^{3+}/Ni^{2+} couples would be expected to enhance the conductivity and electrochemical properties of the LSFN sample.

The electrical conductivity for $Sr_3Fe_2O_{7-\delta}$sample increases to a peak of about 60.4 S·cm^{-1} at around 500 °C, and then reduces as the temperature increases from 300 °C to 800 °C as shown in Fig. 3, exhibiting typical semi-conductor-like behavior[19, 20]. Fig. 3 also gives the electronic conductivity of LSFN sample measured at 300-800 °C in air, and LSFN sample presents typical metallic behavior as well as $La_3Ni_2O_{7-\delta}$, of which the conductivities increase with the decrease of temperatures (223 S·cm^{-1} at 300°C[27]). The charge carriers, Fe^{3+} /Fe^{4+} and Ni^{3+} /Ni^{2+} redox couples, directly affect the change from the semiconductor-like to metallic conducting behavior, indicating that Ni doping into Fe-site causes the 3d electron delocalized [21, 22]. Therefore, LSFN sample presents improved conductivity and is superior to both $Sr_3Fe_2O_{7-\delta}$ and $La_3Ni_2O_{7-\delta}$.

Before the electrochemical performance of LSFN single-phase and composite cathode for anode supported PCFCs was measured, the chemical compatibility behavior of LSFN-BZCY mixture was evaluated. LSFN-BZCY mixture with the same mass calcined in air at 800-1100 °C for 10h, respectively. There are no any reaction between LSFN and BZCY before 1000°C as shown in Fig. 4. Although a small amount of (BaSr)$FeO_{3-\delta}$ was observed, the vast majority of the LSFN-BZCY composite were very stable after calcined at 1100 °C. Meanwhile, (BaSr)$FeO_{3-\delta}$-based cathode owns high catalytic activity and exhibits excellent electrochemical performance (696 mW·cm^{-2} at 700 °C[34]). Therefore, anode supported PCFCs based on LSFN single-phase and composite cathode have been measured at 650-500°C, and I-V-P

curves were given in Fig. 5. The open-circuit voltage values of LSFN and LSFN-BZCY at 650°C are 1.02 and 1.04 V, indicating the highly dense microstructure of BZCY electrolyte. The maximum power densities of LSFN single-phase cathode are 348.0, 219.6, 136.2, and 71.7 $mW{\cdot}cm^{-2}$ at 650, 600, 550 and 500°C. With the incorporation of BZCY, the maximum power densities of LSFN-BZCY composite cathode increase to 426.0, 332.3, 188.8, and 94.5 $mW{\cdot}cm^{-2}$ at the same operation temperature. Obviously, LSFN-BZCY composite cathode exhibits much higher performance than Co-doped $La_3Ni_2O_{7-\delta}$ (*398* $mW{\cdot}cm^{-2}$[27]), but still lower than $Sr_3Fe_2O_{7-\delta}$-5wt.%BZCY composite cathode (*583* $mW{\cdot}cm^{-2}$[19]).

To evaluate the catalytic performance of LSFN-BZCY composite cathode for oxygen reduction reactions, electrochemical impedance spectroscopy (EIS) measurements was used to perform anode supported PCFCs under open-circuit conditions as shown in Fig.6 (a). Electrode polarization resistance (Rp) and the ohmic resistance (Rb) can be calculated from the impedance as well as the total resistance (Rt), and then presented in Fig. 6(b). Temperature has a significant effect on the Rp and Ro at the working temperatures, and the Rp value increased from 0.26 to 1.72 $\Omega{\cdot}cm^2$ with the reduce temperature, while corresponding Rb only changes from 0.47 to 1.23 $\Omega{\cdot}cm^2$, indicating that the Rp is the rate-limiting step for PCFCs at low temperatures. LSFN-BZCY composite cathode exhibits low Rp than Co-doped $La_3Ni_2O_{7-\delta}$(*7.6* $\Omega{\cdot}cm^2$ [27]), but much larger than $Sr_3Fe_2O_{7-\delta}$-5wt.%BZCY composite cathode (*0.15* $\Omega{\cdot}cm^2$ [19]).

As to further detailly investigate the electrode polarization process of anode supported PCFCs with LSFN composite cathode under OCVs conditions, the impedance spectrum analysis using the relaxation time distribution (DRT) method can be characterized as the peaks in the $F(\tau)$vs.-log10($2\pi\tau$) curves as follows [35-38]:

$$F(\tau) = \tau G(\tau)\ln(10) = \frac{-\ln(10)}{\pi}\left[Z''\left(e^{-\ln\tau+\frac{j\pi}{2}}\right) + Z''\left(e^{-\ln\tau-\frac{j\pi}{2}}\right)\right] \qquad (2)$$

where $F(\tau)$ is the distribution function of the relaxation time. As shown in Fig. 7(a), The calculated DRT plots exhibit several polarization processes. It clearly can be seen that there exist three (P1, P2, P3) main peaks at different operation temperatures, suggesting there are three rate-limiting steps. Meanwhile, all the peaks shift to high frequency with the reduced temperatures, suggesting the charge transfer with electron and oxygen-ion at reduced temperature becomes more difficult at the electrode-electrolyte interfaces. Simulated resistances correspond to P1, P2 and P3 are presented in Fig. 7(b, c). P1 observed at the high frequency decreases with the increasing temperature, and therefore P1 is considered to be proton incorporation and diffusion at cathode-electrolyte interface [36, 37]. As can be seen from Fig. 7(b), the proportion of P1 is much larger than P2 and P3, indicating that P1 is the rate-limiting step for the reaction. Since LSFN single-phase cathode has ignorable proton conductivity and the mix of BZCY can dramatically improve the proton conducting behavior. P2 is the processes of H_2 adsorption, dissociation and proton formation at anode and the proportion of P2 is almost the same as temperature reduced. Certainly, P3 also decreases with the increasing temperature and locates at the low frequency. Therefore,

P3 is supposed to oxygen dissociation, adsorption and diffusion in cathode with low proportion of about 19 % at 500°C owing to excellent conductivity of LSFN.

Fig. 8 shows the stability test of LSFN composite cathode with a 50 $mA{\cdot}cm^{-2}$ discharge current density at 700°C in humidified H_2 fuel. The output voltages varied with test time were recorded, and results indicated that the voltage remained a stable value at 0.96 V within 50 h test. Fig. 9(a) shows cross-sectional images of anode-supported PFCFs with LSFN-BZCY cathode after long-term testing. The 30 μm-thickness proton BZCY electrolyte is dense enough and adheres well with LSFN-BZCY cathode under the cover of silver, preventing the gas leakage and ensuring efficient proton transmission. Besides, there are countless microporous at the approximate 35μm-thick anode functional layer from the reduction of NiO and macroporous at anode substrate as shown in Fig. 9(b), leading to a better interfacial contact between anode substrate and electrolyte. Preliminary results demonstrated new two-layer RP structure LSFN must be a promising cathode candidate for PCFCs, and catalytic activity and proton conductivity of LSFN single-phase cathode can be further enhanced by incorporation with BZCY.

4. Conclusions

In this work, we successfully synthesized two-layer Ruddlesden-popper oxide $La_{0.25}Sr_{2.75}FeNiO_{7-\delta}$ (LSFN) and then was evaluated as the active single-phase and composite cathode for proton ceramics fuel cells (PCFCs). LSFN with the tetragonal symmetrical structure (I4/mmm) is confirmed by the XRD Rietveld refinement. Furthermore, the XPS results obviously prove the co-existence of Fe^{3+} /Fe^{4+} and Ni^{3+}/Ni^{2+} couples in the combination of two RP phase oxides of $Sr_3Fe_2O_{7-\delta}$ and $La_3Ni_2O_{7-\delta}$, and directly affect the change from the semiconductor-like to metallic conducting behavior confirmed by the conductivity measurement. Importantly, anode supported PCFCs using LSFN-BZCY cathode achieved maximum power densities of 426.0, 332.3, 188.8, and 94.5 $mW{\cdot}cm^{-2}$ at 650 – 500°C, respectively, with corresponding Rp of 0.29, 0.43, 0.79, and 1.72 $\Omega{\cdot}cm^2$. The electrode polarization processes were further analyzed using the relaxation time distribution function (DRT), and thus three polarization peaks (P1, P2, P3) observed in DRT curves shifted to the right at high frequency with the decreasing temperature, suggesting that the charge transfer at the electrode-electrolyte interfaces become more difficult at reduced temperature. Preliminary results demonstrated two-layer RP structure LSFN can be a promising cathode candidate for PCFCs.

Declarations

Acknowledgements

The authors would like to thank the financial support from the National Natural Science Foundation of China (No. 51602343).

References

1. Radenahmad N, Afif A, Petra PI et al (2016) Proton-conducting electrolytes for direct methanol and direct urea fuel cells - a state-of-the-art review. Renew Sust Energ Rev 57:1347–1358
2. Duan C, Kee RJ, Zhu H et al (2018) Highly durable, coking and sulfur tolerant, fuel-flexible protonic ceramic fuel cells. Nature 557:217–222
3. Bonanos N, Huijser A, Poulsen FW (2015) H/D isotope effects in high temperature proton conductors. Solid State Ionics 275:9–13
4. Fabbri E, Pergolesi D, Traversa E (2010) Materials challenges toward proton-conducting oxide fuel cells: a critical review. Chem Soc Rev 39:4355–4369
5. Yang L, Zuo C, Wang S et al (2008) A novel composite cathode for low-temperature SOFCs based on oxide proton conductors. Adv Mater 20:3280–3283
6. Lashtabeg A, Skinner SJ (2006) Solid oxide fuel cells - a challenge for materials chemists. J Mater Chem 16:3161–3170
7. Shao Z, Haile SM (2004) A high-performance cathode for the next generation of solid-oxide fuel cells. Nature 35:170–173
8. Dong F, Chen D, Ran R et al (2012) A comparative study of $Sm_{0.5}Sr_{0.5}MO_{3-\delta}$ (M = Co and Mn) as oxygen reduction electrodes for solid oxide fuel cells. Int J Hydrogen Energ 37:4377–4387
9. Nie L, Liu M, Zhang Y et al (2010) $La_{0.6}Sr_{0.4}Co_{0.2}Fe_{0.8}O_{3-\delta}$ cathodes infiltrated with samarium-doped cerium oxide for solid oxide fuel cells. J Power Sources 195:4704–4708
10. Zhou W. Shao Z, Ran R et al (2008) A novel efficient oxide electrode for electrocatalytic oxygen reduction at 400–600°C. Chem Commun 44:5791–5793
11. Leng Y, Chan SH, Liu Q (2008) Development of LSCF-GDC composite cathodes for low-temperature solid oxide fuel cells with thin film GDC electrolyte. Int J Hydrogen Energ 33:3808–3817
12. Xia CR, Rauch W, Chen FL et al (2002) $Sm_{0.5}Sr_{0.5}CoO_3$ cathodes for low-temperature SOFCs. Solid State Ionics 149:11–19
13. Mogni L, Fouletier J, Prado F et al (2005) High-temperature thermodynamic and transport properties of the $Sr_3Fe_2O_{6+\delta}$ mixed conductor. J Solid State Chem 178:2715–2723
14. Beppu K, Hosokawa S, Teramura K et al (2015) Oxygen storage capacity of $Sr_3Fe_2O_{7-\delta}$ having high structural stability. J Mater Chem A 3:13540–13545
15. Yashima M, Enoki M, Wakita T, et al. **Structural disorder and diffusional pathway of oxide ions in a doped Pr_2NiO_4-based mixed conductor**. J. Am. Chem. Soc. 2008, **130**:**2762–2763**.
16. Tarancon A, Skinner S.J, Chater RJ, et al. **Layered perovskites as promising cathodes for intermediate temperature solid oxide fuel cells**. J. Mater. Chem. 2007,**17**:**3175–3181**.
17. Patrakeev MV, Leonidov IA, Kozhevnikov VL et al (2004) Ion-electron transport in strontium ferrites: relationships with structural features and stability. Solid State Sci 6:907–913
18. Ling Y, Wang F, Budiman RA et al (2015) Oxygen nonstoichiometry, the defect equilibrium model and thermodynamic quantities of the Ruddlesden-Popper oxide $Sr_3Fe_2O_{7-\delta}$. PhysChemChemPhys

17:7489–7497

19. Wang ZQ, Yang WQ, Shafi SP et al (2015) A high performance cathode for proton conducting solid oxide fuel cells. J Mater Chem A 3:8405–8412
20. Ling YH, Guo TM, Zhang XZ et al (2017) Evaluation of electrical conductivity and oxygen diffusivity of the typical Ruddlesden-Popper oxide $Sr_3Fe_2O_{7-\delta}$. Ceram Int 43:16264–16269
21. Mogni L, Prado F, Ascolani H et al (2005) Synthesis, crystal chemistry and physical properties of the Ruddlesden-Popper phases $Sr_3Fe_{2-x}Ni_xO_{7-\delta}$($0 < x < 1.0$). J Solid State Chem 178:1559–1568
22. Mogni L, Prado F, Caneiro A (2006) Defect structure and electrical conductivity of the Ruddlesden-Popper phases $Sr_3FeMO_{6+\delta}$(M = Co, Ni). Chem Mater 18:4163–4170
23. Ling YH, Wang F, Okamoto Y et al (2016) Oxygen nonstoichiometry and thermodynamic quantities in the Ruddlesden–Popper oxides $La_xSr_{3-x}Fe_2O_{7-\delta}$. Solid State Ionics 288:298–302
24. Ling YH, Wang F, Okamoto Y et al (2016) Oxygen nonstoichiometry and thermodynamic explanation of large oxygen-deficient Ruddlesden–Popper oxides $La_xSr_{3-x}Fe_2O_{7-\delta}$. J Am Ceram Soc 99:3792–3801
25. Yoo S, Choi S, Shin J et al (2012) Electrical properties, thermodynamic behavior, and defect analysis of $La_{n+1}Ni_nO_{3n+1+d}$ infiltrated into YSZ scaffolds as cathodes for intermediate-temperature SOFCs, Rsc. Adv 2:4648–4655
26. Amow G, Davidson I, Skinner SA (2006) A comparative study of the Ruddlesden-Popper series, $La_{n+1}Ni_nO_{3n+1}$ (n = 1, 2 and 3), for solid-oxide fuel-cell cathode applications. Solid State Ionics 177:1205–1210
27. Chen ZZ, Wang JL, Huan DM et al (2017) Tailoring the activity via cobalt doping of a two-layer Ruddlesden-Popper phase cathode for intermediate temperature solid oxide fuel cells. J Power Sources 371:41–47
28. Ling YH, Lu XY, Niu JN et al (2016) Antimony doped barium strontium ferrite perovskites as novel cathodes for intermediate-temperature solid oxide fuel cells. J Alloy Compd 666:23–29
29. Velazquez-Palenzuela A, Zhang L, Wang LC et al (2011) Carbon-Supported Fe-Nx catalysts synthesized by pyrolysis of the Fe(II)-2,3,5,6-tetra(2-pyridyl)pyrazine complex: structure, electrochemical properties, and oxygen reduction reaction activity. J Phys Chem C 115:12929–12940
30. Xiao GL, Liu Q, Wang SW et al (2012) Synthesis and characterization of Mo-doped $SrFeO_{3-\delta}$ as cathode materials for solid oxide fuel cells. J Power Sources 202:63–69
31. Dai N, Feng J, Wang Z et al (2013) Synthesis and characterization of B-site Ni-doped perovskites $Sr_2Fe_{1.5-x}Ni_xMo_{0.5}O_{6-\delta}$ (x = 0, 0.05, 0.1, 0.2,0.4) as cathodes for SOFCs. J Mater Chem A 1:14147–14153
32. Kang HW, Lim SN, Park SB (2012) Co-doping schemes to enhance H_2 evolution under visible light irradiation over $SrTiO_3$:Ni/M (M = La or Ta) prepared by spray pyrolysis. Int J Hydrogen Energ 37:5540–5549

33. Lu YX, Jiang Y, Yang Z et al (2013) ChemInform abstract: polymer-assisted synthesis of $LiNi_{2/3}Mn_{1/3}O_2$ cathode material with enhanced electrochemical performance. J Alloy compd 559:203–208
34. Sun WP, Shi Z, Fang SM et al (2010) A high performance $BaZr_{0.1}Ce_{0.7}Y_{0.2}O_{3-\delta}$-based solid oxide fuel cell with a cobalt-free $Ba_{0.5}Sr_{0.5}FeO_{3-\delta}–Ce_{0.8}Sm_{0.2}O_{2-\delta}$ composite cathode. Int J Hydrogen Energ 35:7925–7929
35. Fuoss RM, Kirkwood JG (2002) Dipole moments in polyvinyl chloride-diphenyl systems, electrical properties of solids. VIII. Dipole moments in polyvinyl chloride-diphenyl systems. J Am Chem Soc 63:385–394
36. Shi N, Su F, Huan DM et al (2017) Performance and DRT analysis of P-SOFCs fabricated using new phase inversion combined tape casting technology. J Mater Chem A 5:19664–19670
37. Zheng D, Han X (2017) Numerical investigation of coupled mass transport and electrochemical reactions in porous SOFC anode microstructure. Int J Heat Mass Transfer 109:1252–1260
38. Cai W, Guo YY, Zhang T, et al. **Characterization and polarization DRT analysis of a stable and highly active proton-conducting cathode**. Ceram. Int. 2018, **44**:**14297–14302**.

Figures

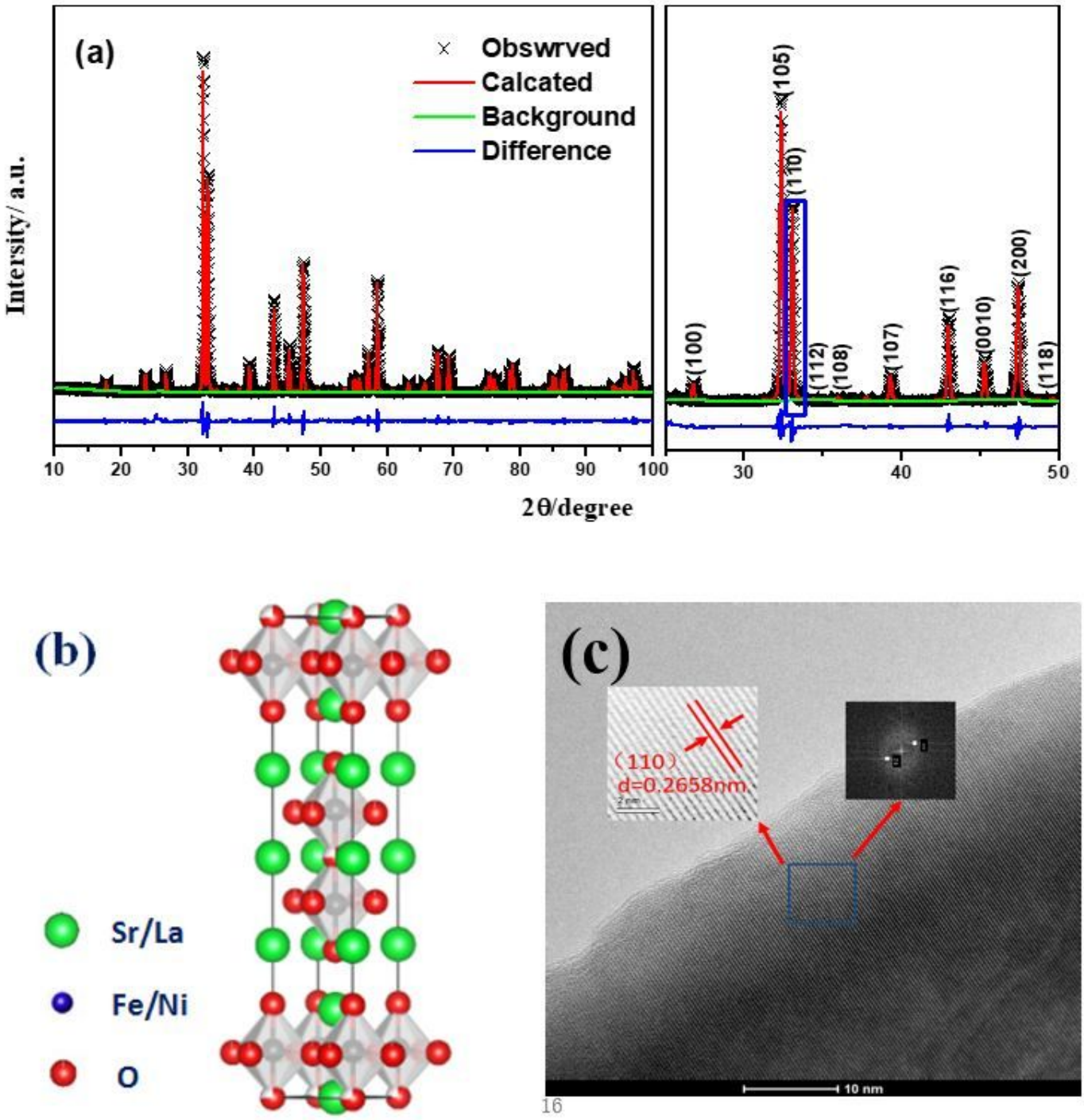

Figure 1

(a) Rietveld refinement data for LSFN powder prepared though EDTA- citric acid combustion method, and calcined at 1200 °C-3 h(magnified results with 2θ of 25-50 °), (b) the typical two-layer Ruddlesden-Popper phase structure, and (c) high-resolution TEM image of LSFN samples;

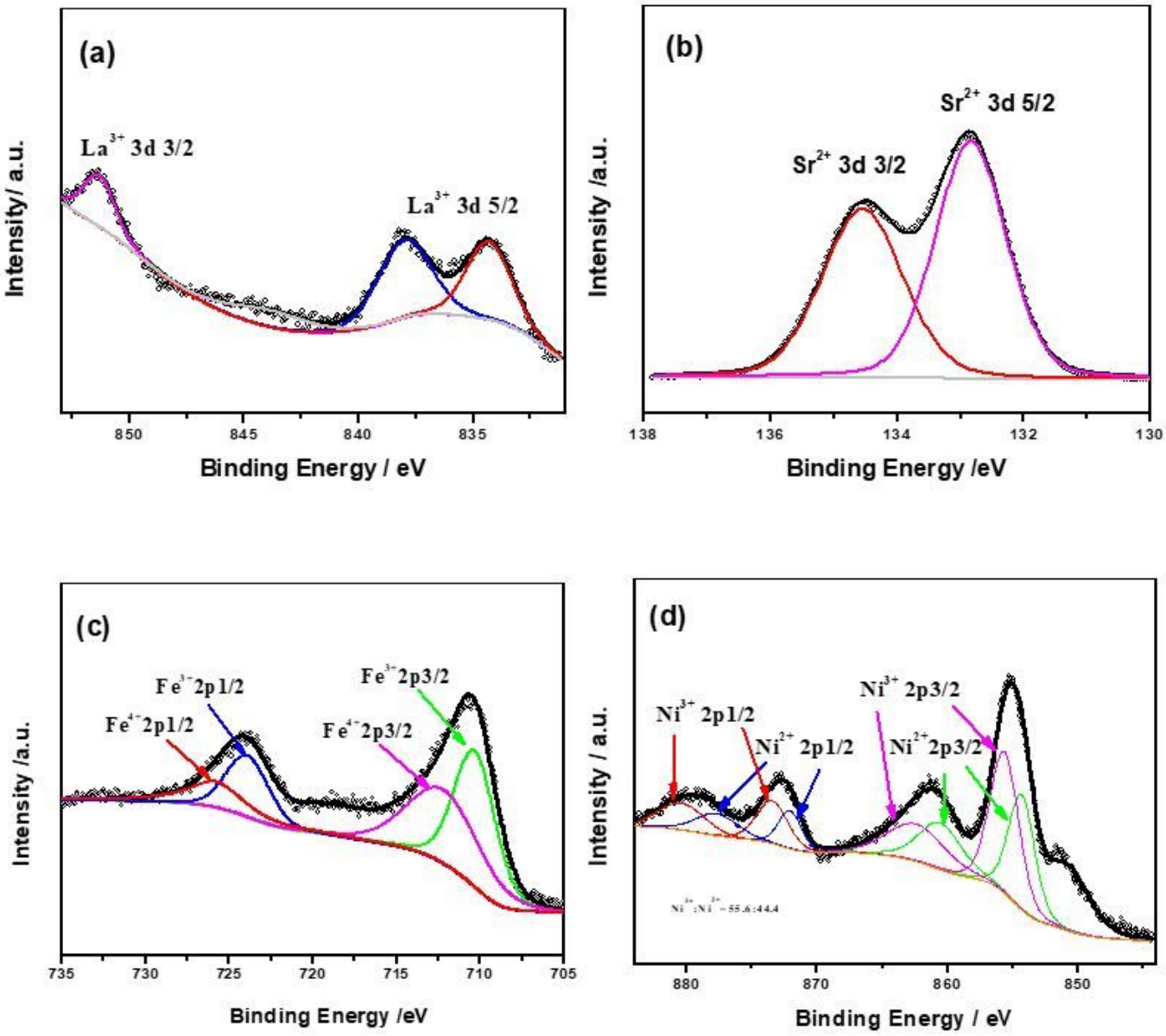

Figure 2

XPS spectra at room temperature for (a) La3d, (b)Sr3d, (c) Fe 2p and (d) Ni2p of LSFN sample;

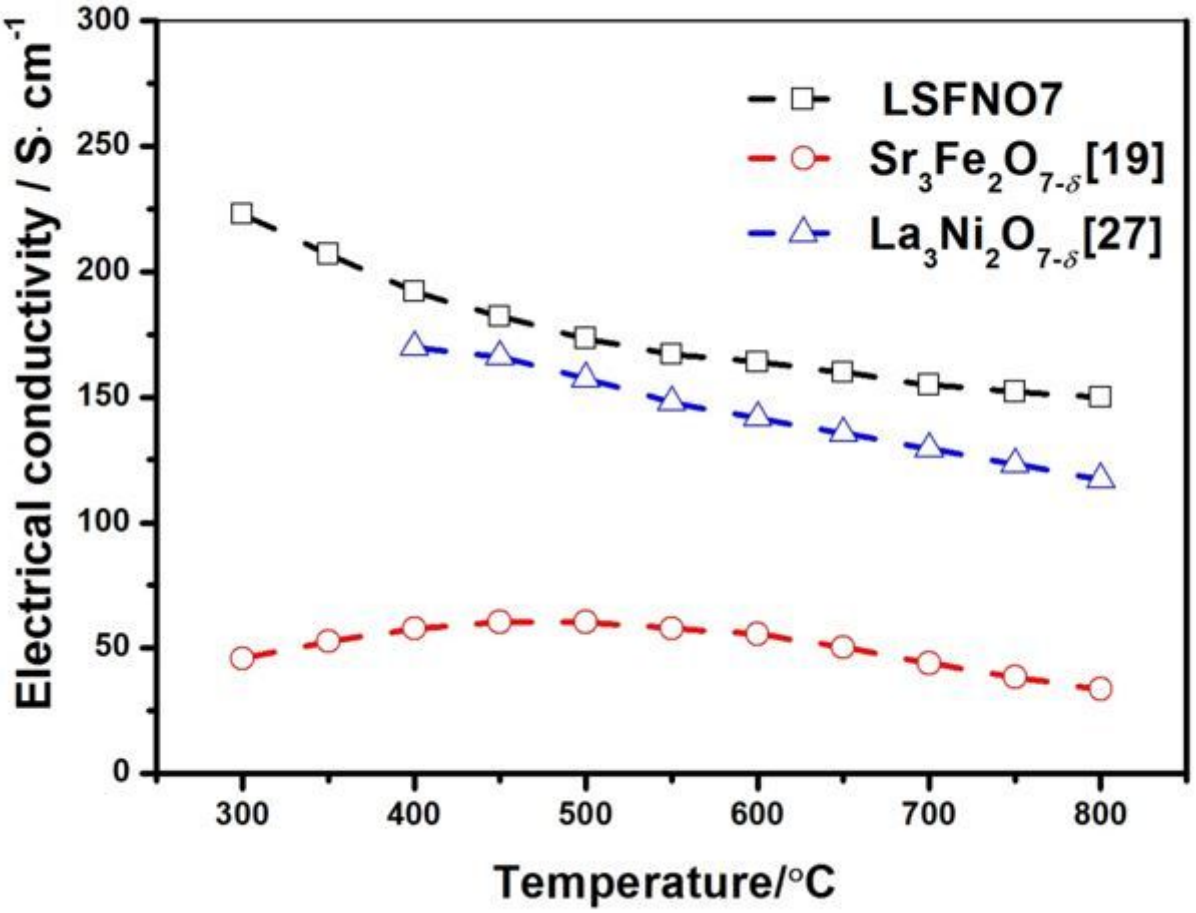

Figure 3

Temperature dependence on conductivity for LSFN in air, and Sr3Fe2O7-δ and La3Ni2O7-δ conductivity data from the literatures [19, 27].

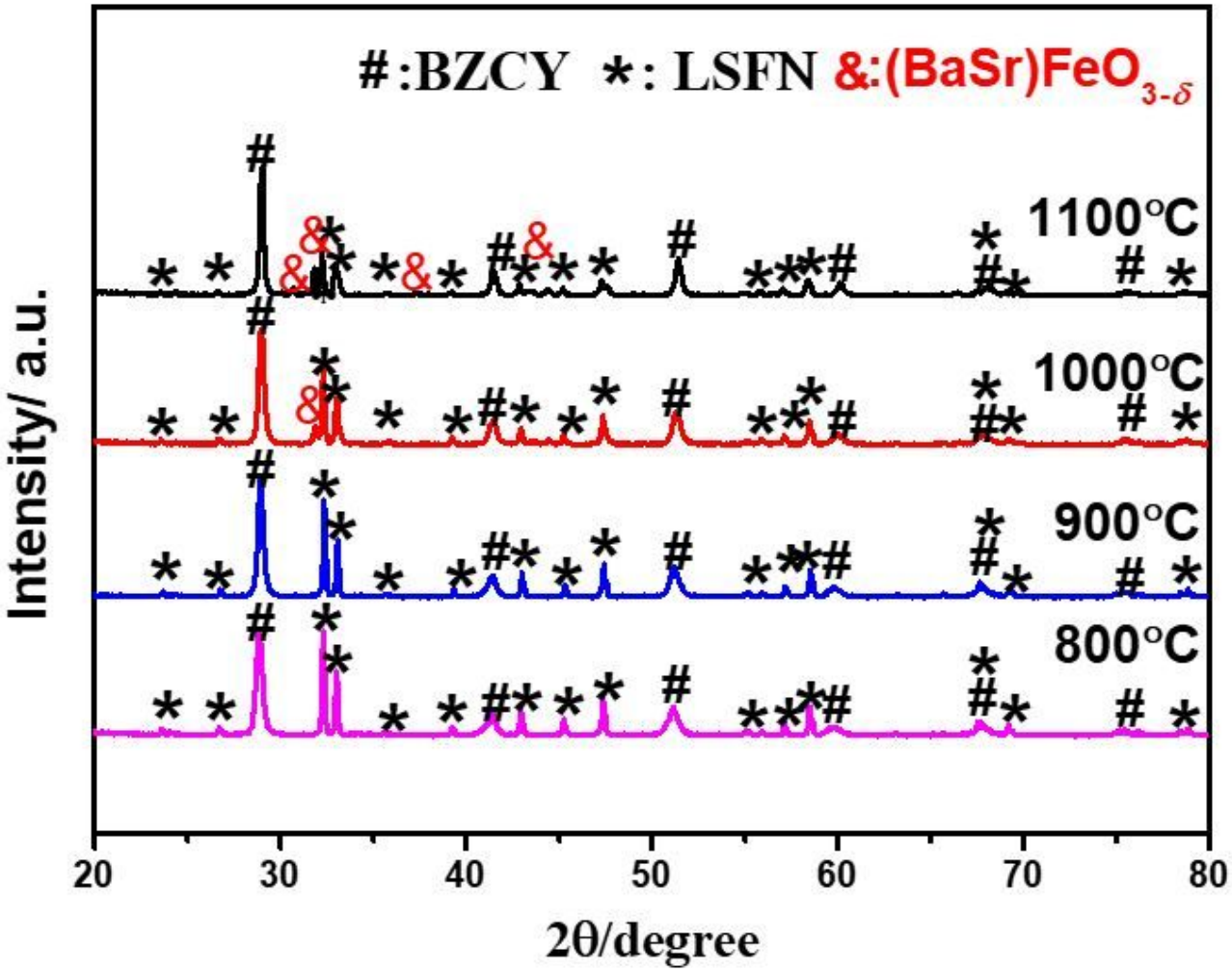

Figure 4

XRD patterns of LSFN-BZCY mixture calcined at 800-1100°C for 10h, respectively.

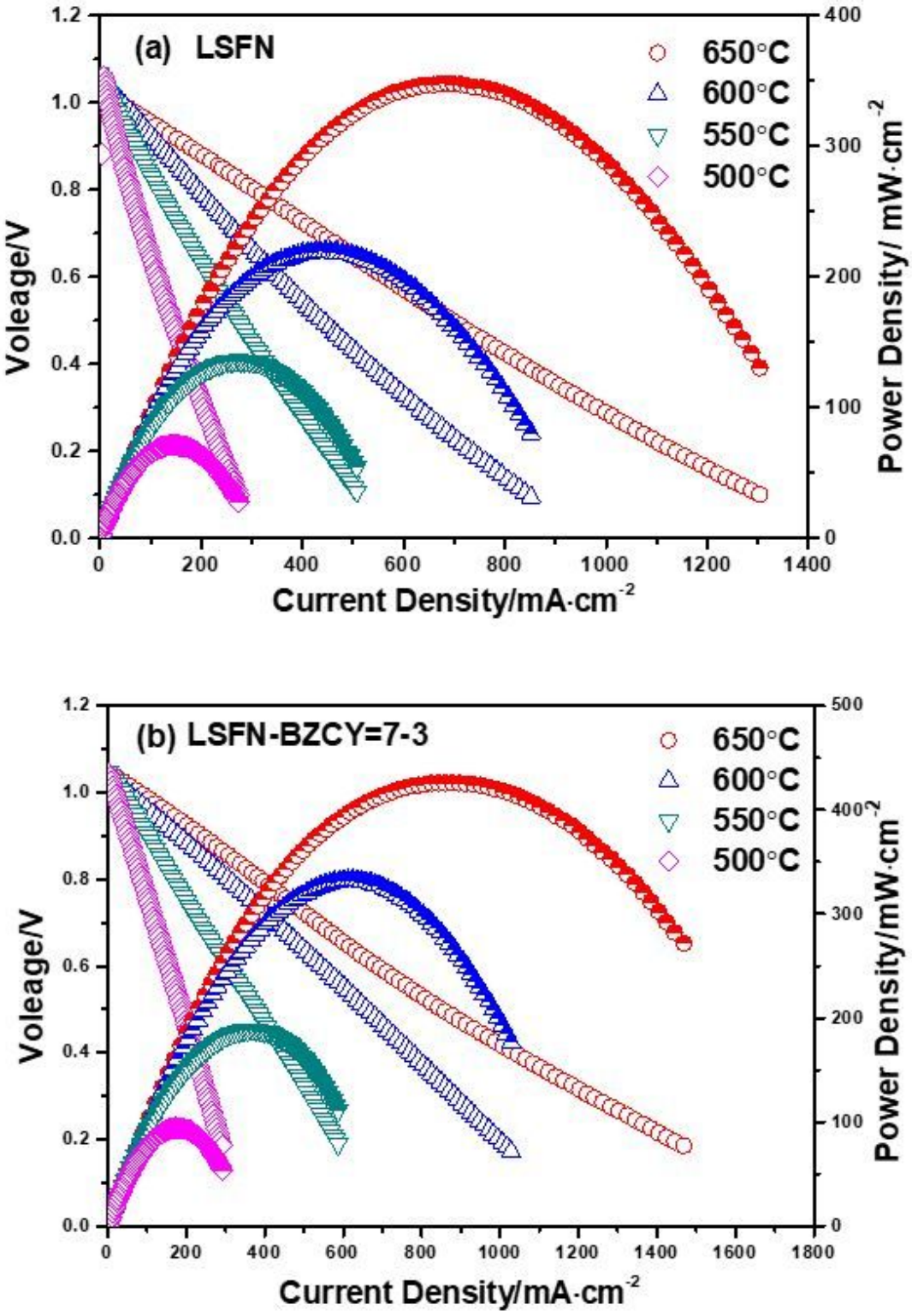

Figure 5

I-V-P curves of anode supported PCFCs with LSFN single-phase cathode (a) and LSFN-BZCY composite cathode (b) measured from 650 to 500 °C.

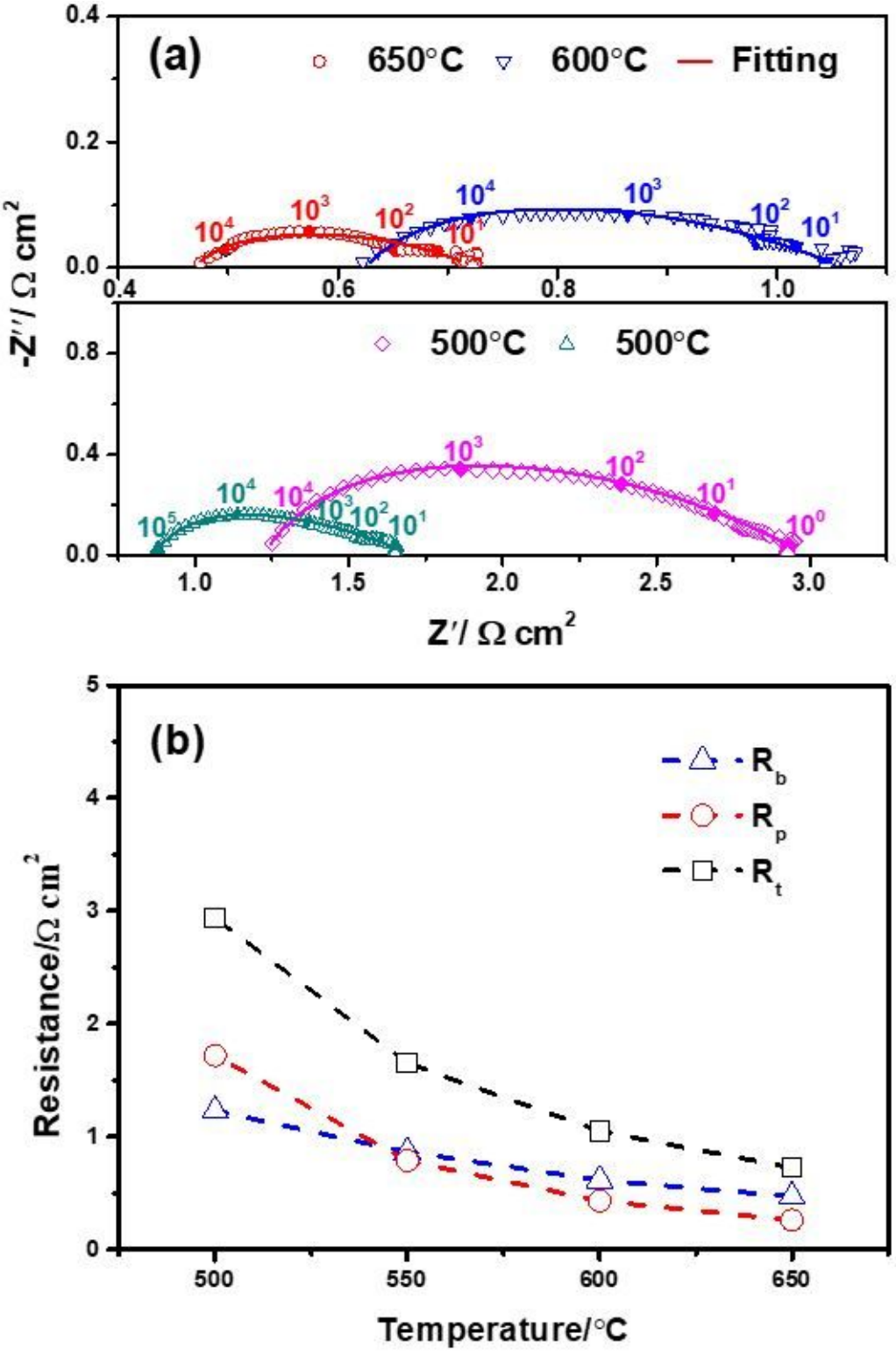

Figure 6

(a) Impedance spectra for anode supported PCFCs with LSFN-BZCY composite cathode measured under open-circuit conditions from 650°C to 500°C, and (b)the temperature dependence of electrode interfacial polarization resistance (Rp), ohmic resistance (Ro), and total resistance (Rt).

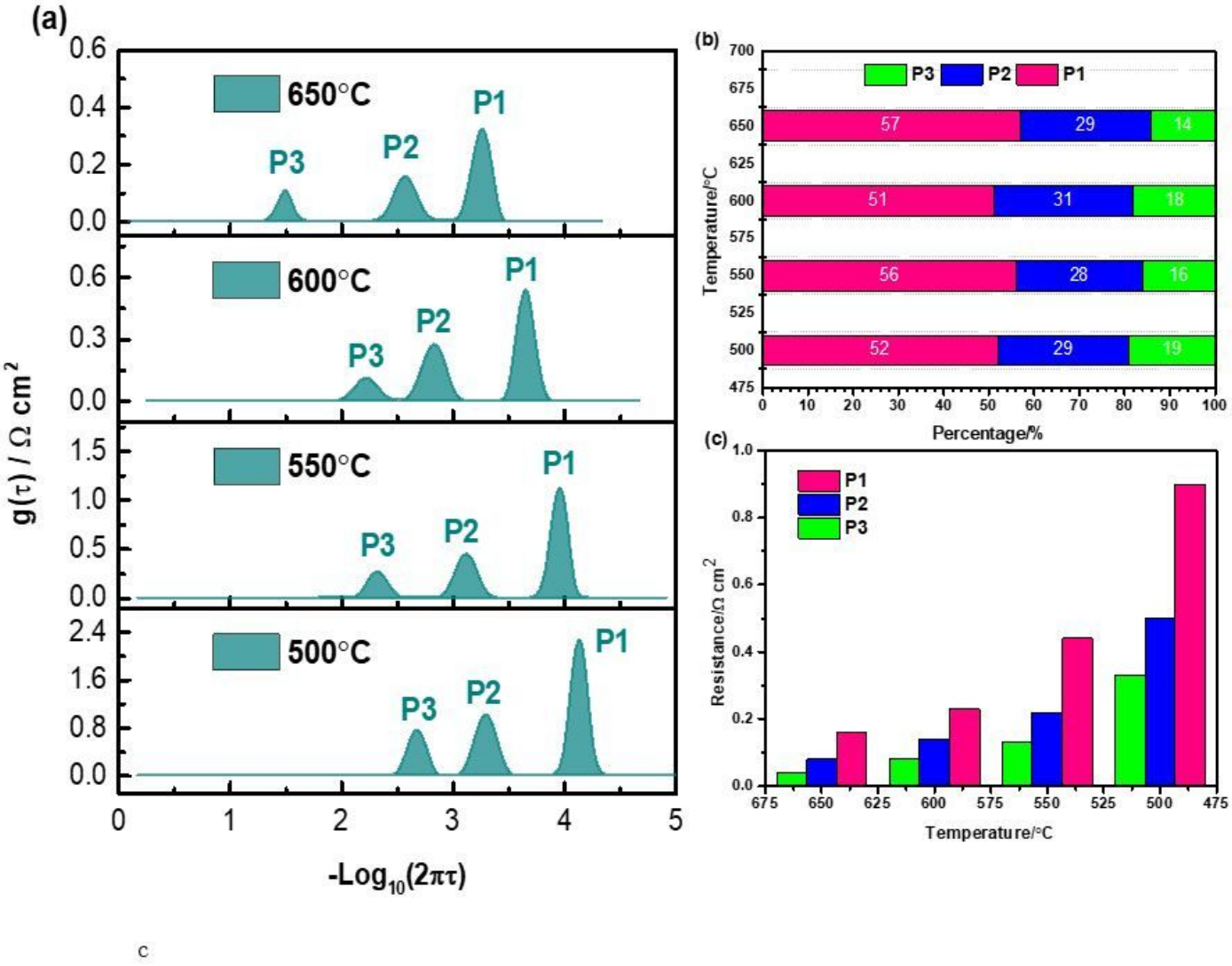

c

Figure 7

DRT analysis results of the impedance spectra under open-circuit conditions from 650°C to 500°C, and (b, c) Simulated resistances of P1, P2 and P3 corresponding to each fitted peak.

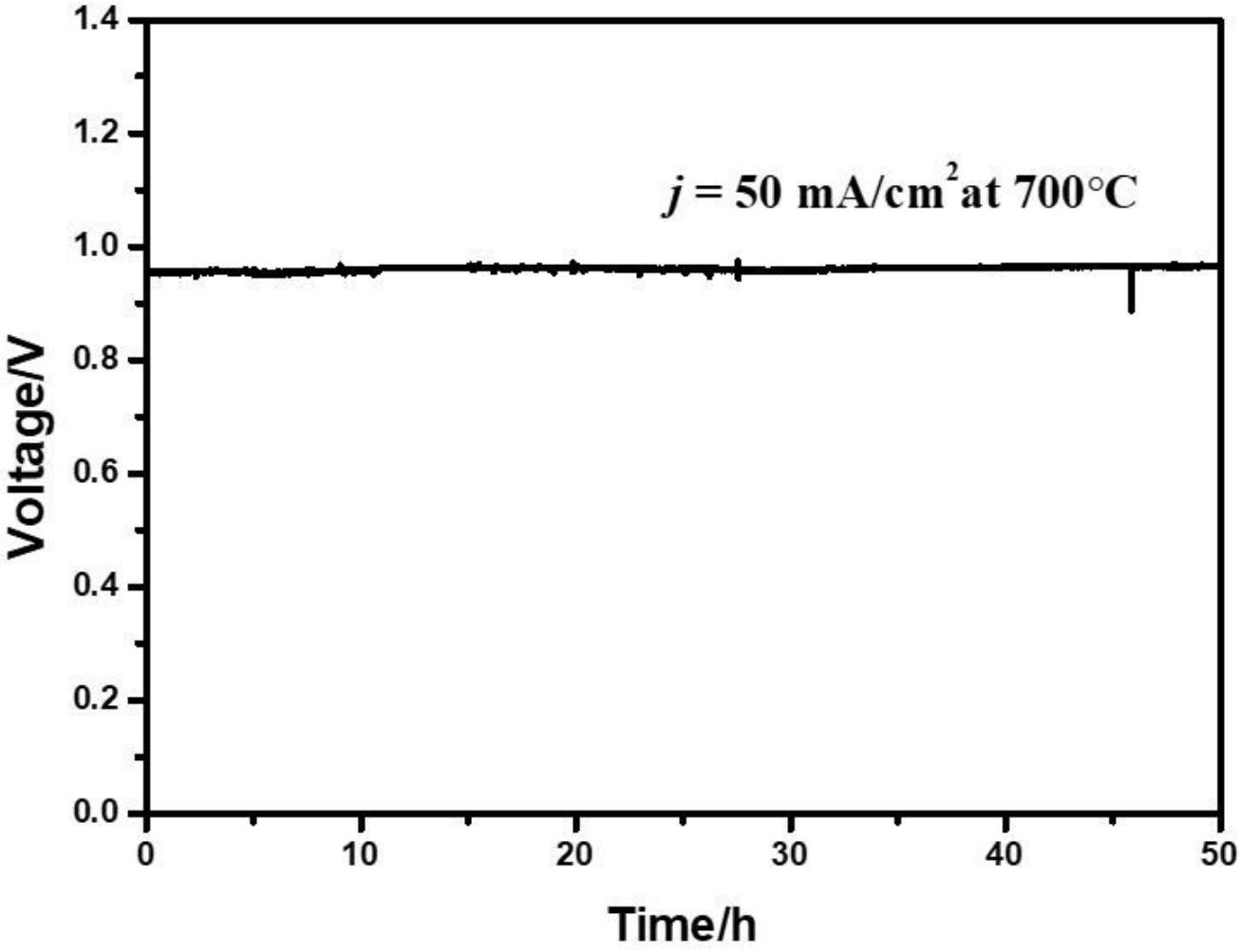

Figure 8

Long-term stability of anode supported PCFCs with LSFN-BZCY composite cathode with the applied discharge current density of 50 mA cm-2 at 700°C.

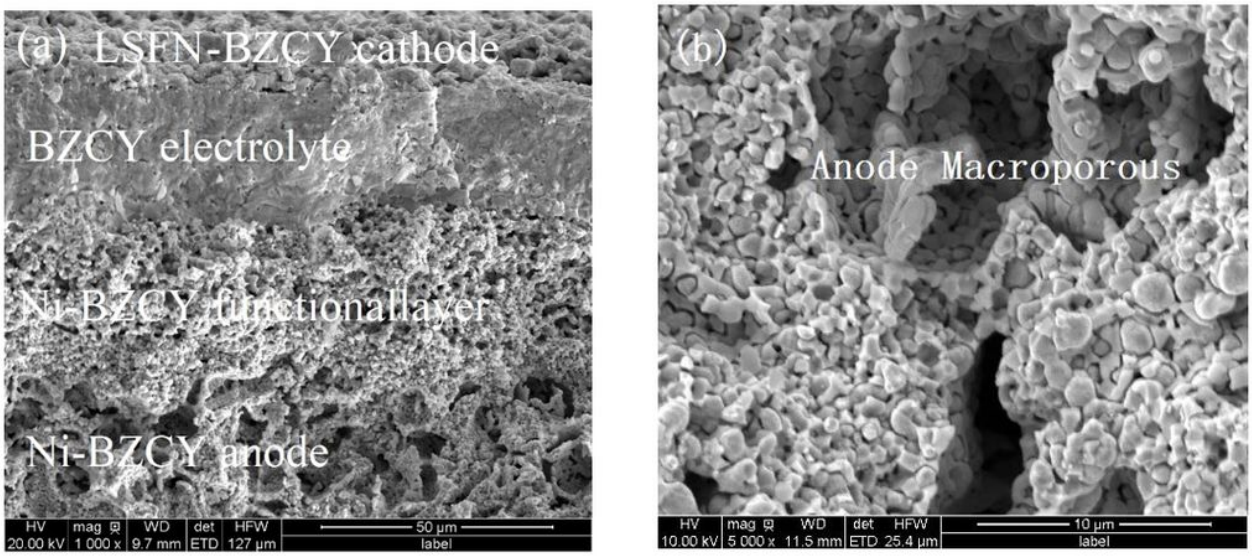

Figure 9

SEM images of anode supported PCFCs with LSFN single-phase cathode (a)cross-section and (b) Ni-BZCY anode substrate